

Simultaneous blockade of two remote magnons induced by an atomYe-Ting Yan, Chengsong Zhao, Da-Wei Wang, Junya Yang, and Ling Zhou ^{*}*School of Physics, Dalian University of Technology, Dalian 116024, China*

(Received 27 October 2023; accepted 16 January 2024; published 13 February 2024)

In this paper, we present a scheme to simultaneously blockade two remote magnons by coupling them to an odd-number cavity array. In the system, a two-level atom is contained in the middle cavity and two Yttrium iron garnet (YIG) spheres are placed in the symmetrical cavity to the atom. By eliminating the cavity array, a master equation with the effective coherent and dissipative couplings among the two magnons and the atom is obtained. When the frequency of the atom is outside the cavity photon band, the dissipative couplings disappear, and only coherent couplings survive, but the effective dispersive coupling strength decreases rapidly with the increasing of the distance between two YIG spheres. When the frequency of the atom is inside band, although the induced dissipation cannot be eliminated, the dissipative coupling and the coherent coupling between two YIG spheres can coexist for long distance. We further show that, under the condition of single excitation resonance, the simultaneous blockade of two remote magnons can be obtained, but the thermal noise of the magnon and atom is still required to be depressed. Thus, by coupling a local two-level atom to a cavity array, we can simultaneously blockade two remote magnons, which provides us an effective method to manipulate remote YIG spheres.

DOI: [10.1103/PhysRevA.109.023710](https://doi.org/10.1103/PhysRevA.109.023710)**I. INTRODUCTION**

Blockade is one of the effective methods to generate a single excitation source and also an important property of the quantum system. The mechanisms of photon blockade can be classified as the single excitation resonant mechanism, conventional and unconventional mechanisms. The single excitation resonant mechanism of photon blockade results from the two-level emitter resonantly interacting with the cavity field [1–5]. The blockade resulting from Kerr nonlinearity strength is called the conventional photon blockade mechanism, which requires nonlinearity strength to be at least larger than the cavity linewidth [6–8]. Unconventional photon blockade can be generated through destructive interference, which can overcome the requirement of strong Kerr nonlinearity of conventional mechanism and has attracted a lot of attention [9–16].

In recent years, hybrid quantum systems based on magnons have been developed rapidly such as cavity optomagnonics [17–20], cavity magnomechanics [21,22], and hybrid ferromagnetic-superconducting systems [23–25]. Since strong and ultrastrong coupling can be generated between magnons and microwave photons in a superconducting cavity [26–30], employing the magnon to manipulate quantum information attracted attention, therefore the blockade of magnons so as to generate a single magnon becomes an important issue. In analogy to photon blockade, magnon blockade is a phenomenon in which the first magnon excitation in a magnon mode blocks the generation of the second magnon excitation. Much attention has been paid to magnon blockade [31–41]. In [38], a Yttrium iron garnet (YIG) sphere and a transmon superconducting qubit are installed in a microwave cavity and magnon blockade is realized by single excitation resonance.

In [39], the magnon blockade effect was achieved in a non-linear \mathcal{PT} -symmetric-like cavity magnomechanical system. Through jointing conventional and unconventional mechanisms, magnon blockade can be obtained in a three-level atomic ensemble and a YIG sphere coupled to a microwave cavity system [40], simultaneous blockade of the photon-phonon-magnon can be received in a two-level atom and YIG sphere coupling to an optomechanical cavity system [41].

In a closed and conservative system, the interaction between subsystems described by the Hamiltonian is called coherent coupling. If an effective coupling between two subsystems is obtained by coupling them to a common environment, the indirect effective coupling is of Lindblad form or non-Hermitian form and is called dissipative coupling. For example, two cavities coupled to the common environment lead to a dissipative coupling between the two cavities [42]. Dissipative magnon-photon coupling was experimentally proved in [43]. The traveling wave responsible for magnon-photon dissipative coupling results in the generation of level attraction [44]. In addition, long-range coherent and dissipative coupling between two spatially separated magnets was experimentally and theoretically investigated [45]. Furthermore, it was revealed that the cooperative effect of coherent and dissipative magnon-photon couplings lead to nonreciprocity [46] and a unidirectional spin-wave amplifier [47]. Dissipative coupling in the spin exchange system exhibits exceptional points [48], and non-Hermitian topological magnonics was summarised in [49]. More importantly, a coupled-cavity array consisting of N linearly coupled superconducting transmission line cavities has been theoretically investigated [50] and was realized in experiments [51–53]. In addition, the remote magnon-magnon coherent coupling was observed in the two YIG spheres coupled to the transmission line system [54], which pushed the hybrid cavity-magnon system toward constructing a quantum network further. Whether we can employ the

^{*}zhllhxn@dlut.edu.cn

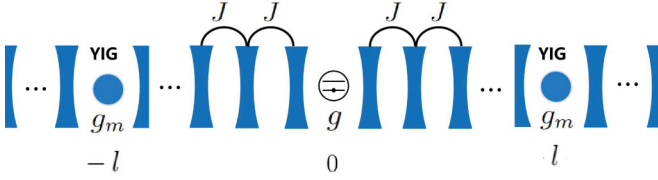


FIG. 1. A schematic of the system where two YIG spheres and one two-level atom are coupled to the cavity array with N coupled resonators.

cavity-magnon system to manipulate remote magnons by local atom deserves our attention.

In this paper, we present a scheme to simultaneously blockade two remote magnons by coupling them to an odd number of cavity arrays where an atom is contained in the middle cavity and two YIG spheres are placed symmetrically to the atom. By eliminating the cavity array, the effective coherent and dissipative couplings among the two magnons and the atom are obtained. When the frequency of the atom is outside the cavity photon band, the dissipative couplings disappear, and only coherent couplings survive, thus putting an atom in the middle of two magnons is equivalent to coupling a giant atom to them, but the effective dispersive couplings decrease rapidly with the increasing of the distance between two YIG spheres. Fortunately, when the frequency of the atom is inside the band, although the induced dissipation cannot be eliminated, the dissipative coupling and the coherent coupling can coexist for remote two YIG spheres. We further show that, under the condition of single excitation resonance, the simultaneous blockade of two remote magnons can be reached, but the magnetic and atomic thermal noise is still required to be depressed.

II. SYSTEM AND THE MASTER EQUATION

As shown in Fig. 1, we consider an odd-number cavity array. A two-level atom is contained in the central cavity, two YIG spheres are placed in the left-side cavity “ $-l$ ” and the right-side cavity “ l ”, respectively, such that the two YIG spheres are symmetry to the atom. The total Hamiltonian is

$$\begin{aligned}
 H = & \omega_c \sum_n a_n^\dagger a_n + \omega_m \sum_{i=-l,l} m_i^\dagger m_i + \omega_a \sigma_+ \sigma_- \\
 & - J \sum_n (a_n^\dagger a_{n+1} + a_{n+1}^\dagger a_n) + [g_m (m_{-l}^\dagger a_{-l} + m_l^\dagger a_l) \\
 & + g \sigma_- a_0^\dagger + \Omega \sigma_- e^{i\omega_p t} + \text{H.c.}], \quad (1)
 \end{aligned}$$

where a_n is the annihilation operator of the cavity at site n with frequency ω_c , and J is the hopping strength between the nearest cavities. For simplicity, we consider that the two YIG spheres with equal frequency ω_m coupled to the cavity array with the same coupling strength g_m . The atom couples to the cavity “0” with strength g and is pumped by a classical field with frequency ω_p .

Then we perform the Fourier transform $a_k = \frac{1}{\sqrt{N}} \sum_n e^{-ikn} a_n$ with $k \in [-\pi, \pi]$, the Hamiltonian in the

momentum representation is

$$\begin{aligned}
 H_1 = & \sum_k \omega_k a_k^\dagger a_k + \omega_m \sum_{i=-l,l} m_i^\dagger m_i + \omega_a \sigma_+ \sigma_- \\
 & + [g_m (m_{-l}^\dagger E_{-l} + m_l^\dagger E_l) + g \sigma_- E_0^\dagger \\
 & + \Omega \sigma_- e^{i\omega_p t} + \text{H.c.}], \quad (2)
 \end{aligned}$$

where $\omega_k = \omega_c - 2J \cos(k)$ is the dispersion relation, which indicates ω_k centered at ω_c with bandwidth $4J$, i.e., ω_k is within $\omega_c \pm 2J$. $E_n = \frac{1}{\sqrt{N}} \sum_k e^{ikn} a_k$ is the field operator at site n . In the frame rotating with the Hamiltonian $\sum_k \omega_k a_k^\dagger a_k + \omega_p \sum_{i=-l,l} m_i^\dagger m_i + \omega_p \sigma_+ \sigma_-$, we have $H' = H_0 + H_{\text{drive}} + H_{\text{int}}$ with

$$H_0 = \sum_{i=-l,l} \Delta_m m_i^\dagger m_i + \Delta_a \sigma_+ \sigma_-, \quad (3)$$

$$H_{\text{drive}} = \Omega (\sigma_- + \sigma_+), \quad (4)$$

$$\begin{aligned}
 H_{\text{int}} = & g_m [m_{-l}^\dagger E'_{-l}(t) e^{i\omega_p t} + m_l^\dagger E'_l(t) e^{i\omega_p t}] \\
 & + g \sigma_- E_0^\dagger(t) e^{-i\omega_p t} + \text{H.c.}, \quad (5)
 \end{aligned}$$

where $E'_n(t) = \frac{1}{\sqrt{N}} \sum_k e^{ikn} e^{-i\omega_k t} a_k$, $\Delta_j = \omega_j - \omega_p$ ($j = m, a$).

We would like to derive a master equation of the atom and the magnons by tracing over the cavities [55–58]. In the process of eliminating the cavity fields, we temporarily ignore the free Hamiltonian H_0 as well as the classical weak pumping H_{drive} because these terms have no relation with the cavity fields. The propagation of photons inside the waveguide is characterized by the group velocity $v_g(\omega_j) = \frac{\partial \omega_k}{\partial k} |_{\omega_k = \omega_j} = \sqrt{4J^2 - (\delta_j)^2}$ [55], where $\delta_j = \omega_j - \omega_c$ and $j = a, m$. When the relaxation time of the waveguide $\frac{1}{|v_g(\omega_j)|}$ is much smaller than the interaction timescales of the cavity array and atom (magnons) $\frac{1}{g \frac{1}{g_m}}$, i.e., $\{g, g_m\} \ll |v_g(\omega_j)|$, the Born-Markov approximation is valid [55–58]. Thus, when the resonance frequency of the atom and the magnon is close to the edge of the cavity photon band, i.e., $\delta_j \approx 2J$, the group velocity of the excited cavity photons is close to zero, the Born-Markov approximation is invalid. Beyond this region, the Born-Markov approximation is still trustable. We will choose parameters far away from the edge of the cavity band. With the Born-Markov approximation, the master equation is formally written as

$$\dot{\rho}_1 = - \int_0^\infty d\tau \text{Tr}_a \{ [H_{\text{int}}(t), [H_{\text{int}}(t - \tau), \mu \otimes \rho_1]] \}, \quad (6)$$

where μ is the density operator of the coupled-cavity array and ρ_1 is the density operator of the hybrid system after eliminating the coupled-cavity array. After complicated calculations, we have

$$\begin{aligned}
 \dot{\rho}_1 = & \sum_{i,j=-l,l} -iy_{ij} [m_i^\dagger m_j, \rho_1] \\
 & - iq_{00} [\sigma_+ \sigma_-, \rho_1] - iw_{0i} [m_i^\dagger \sigma_- + \sigma_+ m_i, \rho_1] \\
 & + x_{ij} (2m_i \rho_1 m_j^\dagger - m_j^\dagger m_i \rho_1 - \rho_1 m_j^\dagger m_i) \\
 & + s_{0i} (2\sigma_- \rho_1 m_i^\dagger - m_i^\dagger \sigma_- \rho_1 - \rho_1 m_i^\dagger \sigma_- + \text{H.c.}) \\
 & + r_{00} (2\sigma_- \rho_1 \sigma_+ - \sigma_+ \sigma_- \rho_1 - \rho_1 \sigma_+ \sigma_-), \quad (7)
 \end{aligned}$$

where

$$\begin{aligned} x_{ij} &= \text{Re}(A_{ij}), & y_{ij} &= \text{Im}(A_{ij}), \\ s_{0i} &= \text{Re}(B_{0i}), & w_{0i} &= \text{Im}(B_{0i}), \\ r_{00} &= \text{Re}(C_{00}), & q_{00} &= \text{Im}(C_{00}), \end{aligned} \quad (8)$$

with $A_{ij} = \frac{g_m^2 e^{iK|n_i - n_j|}}{\sqrt{4J^2 - \Delta_p^2}}$, $B_{0i} = \frac{gg_m e^{iK|n_0 - n_i|}}{\sqrt{4J^2 - \Delta_p^2}}$, $C_{00} = \frac{g^2}{\sqrt{4J^2 - \Delta_p^2}}$, $i, j = \pm l$, $K = \pi - \arccos(\frac{\Delta_p}{2J})$, and $\Delta_p = \omega_p - \omega_c$ describing the detuning between the driving field and the array. If $|\Delta_p| = 2J$, the expressions A_{ij} , B_{0i} , and C_{00} are infinite. $|\Delta_p| \neq 2J$ is the requirement for Eq. (7). However, Δ_p can be smaller or larger than $2J$ and is called the inside or outside band. In our choice of parameters, the inside band $|\Delta_p| < 2J$ and the outside band $|\Delta_p| > 2J$ also mean the frequency of the atom and the magnon falling inside and outside the band. Therefore, the condition $|\Delta_p| \neq 2J$ avoids the frequency of the atom and the magnon in the edge of the cavity photon band, indicating that the Markov approximation is valid except at the edge of the band. Because $\arccos(\frac{\Delta_p}{2J})$ can be multivalued, therefore, in the numerical calculation, we should choose the values that satisfy the positivity of the master equation. From Eq. (7), we can see that y_{l-l} (y_{-ll}) with the Hamiltonian form stands for the coherent coupling between the two YIG spheres, x_{l-l} (x_{-ll}) with the Lindblad form describing the dissipative coupling induced by the common array. Meanwhile, the atom simultaneously interacts with the two YIG spheres in giant-atom form with the coherent coupling strength w_{0l} (w_{0-l}) and the dissipative coupling strength s_{0l} (s_{0-l}). The two-level atom is of anharmonic energy levels, if the frequency of the two-level is resonant with only a single photon, the absorption of a second photon is blocked because the energy of the two photons is detuning far from resonance. Therefore, single-excitation resonance induced by a two-level atom can offer us a blockade [1–5,59]. In the current system, the atom simultaneously interacts with two YIG spheres in coherent and dissipative coupling form, which can offer us simultaneous blockade of the two YIG modes, we will discuss it in Sec. III. In addition, if we would like to account for the dissipation of the cavity array, we can replace ω_c with $\omega_c - \frac{i\kappa_c}{2}$.

We now discuss the effective coupling coefficients in (8) under two cases, i.e., the detuning Δ_p outside the band and inside the band. For the case of the detuning Δ_p outside the band ($\Delta_p > 2J$ or $\Delta_p < -2J$), we plot the coefficients in Fig. 2, where $\Delta_p = -2150\kappa_m$ and $2J = 1000\kappa_m$, satisfying $|\Delta_p| \gg 2J$. See Fig. 2(a), if $\kappa_c = 0$, the induced dissipation rates $x_{ll} = r_{00} = 0$. For nonzero κ_c , x_{ll} and r_{00} are all not zero. That is to say, the nonzero-induced dissipation rates result from the decay of the cavity array. The on-site frequency shifts y_{ll} and q_{00} are plotted in Fig. 2(b), which show that the values of y_{ll} and q_{00} have no relation with κ_c . The induced effective dissipation coupling coefficient x_{-ll} does relate with κ_c , shown in Fig. 2(c), $x_{-ll} = 0$ for $\kappa_c = 0$, but the coherent coupling y_{-ll} has no relation with κ_c shown in Fig. 2(d); and the maximum possible nonzero dissipation coupling $|x_{-ll}|$ and the coherent coupling $|y_{-ll}|$ for integer n' decrease with the increasing of the distance n' ($n' = |n_{-l} - n_l|$) between the two YIG spheres. The nonzero dissipative coupling between the atom and one of the YIG sphere s_{0l} also results from the decay of the cavity array, see

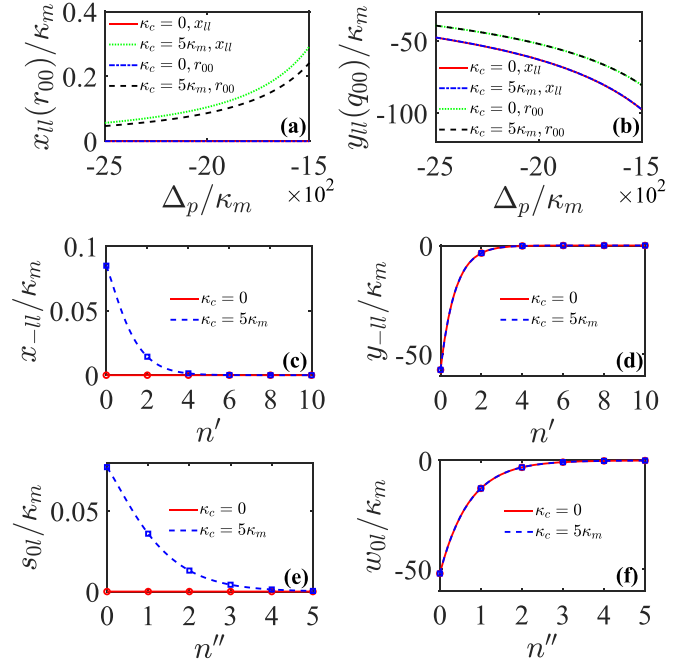


FIG. 2. (a) The effective magnetic dissipation x_{ll} and atomic dissipation r_{00} versus the detuning Δ_p . (b) The magnetic frequency shift y_{ll} and atomic frequency shift q_{00} versus the detuning Δ_p . The effective dissipative coupling (c) x_{-ll} and (e) s_{0l} varying with the distance $n' = |n_{-l} - n_l|$ and $n'' = |n_0 - n_l|$. The effective coherent coupling (d) y_{-ll} and (f) w_{0l} as functions of the distance n' and n'' . For (c)–(f), $\omega_c = 11.4 \times 10^3 \kappa_m$, $\omega_p = 9.25 \times 10^3 \kappa_m$, thus $\Delta_p = -2150\kappa_m$. For all of the plots, $\kappa_m = 1$, $g = 300\kappa_m$, $g_m = 330\kappa_m$, and $J = 500\kappa_m$.

Fig. 2(e), while w_{0l} is not affected by κ_c , and the nonzero maximum possible value $|s_{0l}|$ and $|w_{0l}|$ also decrease with the increasing of n'' ($n'' = |n_0 - n_l|$). One can notice that the induced coherent coupling y_{-ll} and w_{0l} can be larger than κ_m although they decrease with the increasing of distance n' and n'' . We can summarize that if $\kappa_c = 0$, dissipation (x_{ll} , r_{00}) and dissipative coupling (x_{-ll} , s_{0l}) are all zero, only the frequency shift and coherent coupling survive. We can understand it from their mathematical expressions. If $\kappa_c = 0$, $A_{ij} = \pm i \frac{g_m^2 e^{i(\pi - \arccos(\frac{\Delta_p}{2J}))|n_i - n_j|}}{\sqrt{-4J^2 + \Delta_p^2}}$, $B_{0i} = \pm i \frac{gg_m e^{i(\pi - \arccos(\frac{\Delta_p}{2J}))|n_0 - n_i|}}{\sqrt{-4J^2 + \Delta_p^2}}$, $C_{00} = \pm i \frac{g^2}{\sqrt{-4J^2 + \Delta_p^2}}$. Because $\arccos(\frac{\Delta_p}{2J})$ for $\Delta_p > 2J$ is purely imaginary, A_{ij} , B_{0i} , and C_{00} are pure imaginary numbers. When $\Delta_p < -2J$, $\pi - \arccos(\frac{\Delta_p}{2J})$ is a pure imaginary number, then A_{ij} , B_{0i} , and C_{00} are also pure imaginary numbers. Therefore, the real parts of A_{ij} , B_{0i} , and C_{00} are all zero, i.e., x_{-ll} , s_{0l} , x_{ll} , and r_{00} are all zero, and only the imaginary parts y_{-ll} , w_{0l} , y_{ll} , and q_{00} survive, that is to say, the common cavity array induces coherent coupling coefficients y_{-ll} and w_{0l} without the dissipation rates. Physically, when $|\Delta_p| \gg 2J$, due to the frequency of the atom being very close to that of the classical pumping field (which will be analyzed in the next section), the atom actually is far from center frequency ω_c , under this case only dispersively interacts with the cavity array. Therefore, the dispersive interaction does not lead to dissipation as well as dissipative coupling and only induces coherent coupling

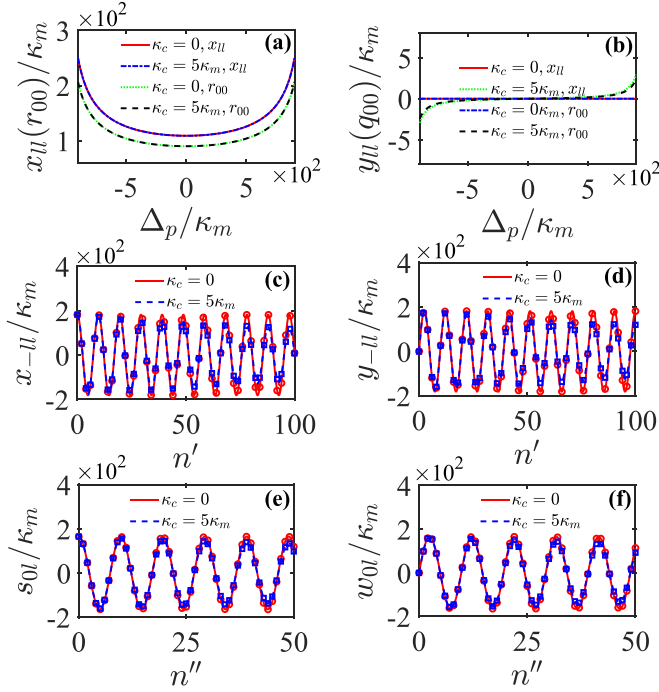


FIG. 3. (a) The effective magnetic dissipation x_{ll} and atomic dissipation r_{00} versus the detuning Δ_p . (b) The magnetic frequency shift y_{ll} and atomic frequency shift q_{00} versus the detuning Δ_p . The effective dissipative coupling (c) x_{-ll} and (e) s_{0l} varying with the distance n' and n'' . The effective coherent coupling (d) y_{-ll} and (f) w_{0l} as functions of the distance n' and n'' . The marked point in (c)–(f) is the case where n' and n'' take all integers. For (c)–(f), $\omega_c = 11.4 \times 10^3 \kappa_m$, $\omega_p = 10.6 \times 10^3 \kappa_m$, thus $\Delta_p = -800 \kappa_m$. For all of the plots, the other parameters are the same as in Fig. 2.

between the atom and the two YIG spheres. Under this condition ($\kappa_c = 0$ and $|\Delta_p| \gg 2J$), from (7) we can write the effective interaction in the form of the effective Hamiltonian as

$$H_{\text{eff}} = \sum_{i=-l,l} y_{ll} m_i^\dagger m_i + q_{00} \sigma_+ \sigma_- + y_{-ll} (m_{-l}^\dagger m_l + m_l^\dagger m_{-l}) + w_{0l} (m_i \sigma_+ + \sigma_- m_i^\dagger). \quad (9)$$

Under this condition, employing the adiabatic elimination method, we can directly derive the same effective Hamiltonian (9), which means that the master equation method equals the adiabatic elimination method for the detuning outside band, and the above derivation and analysis are trustable. Even if the cavity decay is not negligible, the effective coherent couplings are not affected. Therefore, we can safely infer that the triple interaction mediated by the cavity array can finish some quantum processes.

See Figs. 3(a), 3(c), and 3(e), for the detuning inside band (the bandwidth $-2J < \Delta_p < 2J$), different from the case of the outside band, both dissipation x_{ll} (r_{00}) and the dissipative coupling x_{-ll} (s_{0l}) are not zero even with $\kappa_c = 0$. It is reasonable that the resonant or near-resonant interacting with the common environment results in dissipation and the dissipative coupling even without κ_c . The energy shift y_{ll} (q_{00}) and the coherent coupling y_{-ll} (w_{0l}), shown in Figs. 3(b), 3(d), and 3(f), are also affected by κ_c . As shown by the red solid line

in Figs. 3(c)–3(f), for $\kappa_c = 0$, $-2J < \Delta_p < 2J$, $\arccos(\frac{\Delta_p}{2J})$ is a pure real number (K is a real number), the coherent coupling y_{-ll} (w_{0l}) and the dissipative coupling x_{-ll} (s_{0l}) oscillate as functions of n' and n'' rather than pure exponential decreasing like that in Figs. 2(c) to 2(f). Including the dissipation of the cavity array, see the blue dashed lines in Figs. 3(c)–3(f), the maximum values of the coherent and dissipative coupling slightly decrease with n' and n'' . Under this case, Δ_p is substituted by $\Delta_p + i\kappa_c/2$, then K is a complex number whose real part offer us oscillation functions of n' and imaginary part still results in exponential decreasing as function of n' and n'' . Only if the loss of the cavity array is not overlarge ($\{g, g_m\} > \kappa_c$), the coherent coupling y_{-ll} (w_{0l}) and the dissipative coupling x_{-ll} (s_{0l}) oscillating as functions of n' and n'' maybe applicable to long-distance quantum manipulation. The difference in behavior of the coherent coupling y_{-ll} (w_{0l}) and the dissipative coupling x_{-ll} (s_{0l}) between the inside and outside bands is because under near-resonant conditions the excitation transmits along the cavity array so that it can travel long distances, while under dispersion conditions the excitation may not enter into the array so that the induced effective interaction is within a short distance.

III. SIMULTANEOUSLY BLOCKADE THE TWO REMOTE MAGNONS

We are now in the position to discuss the potential application of the current system. See the master equation (7), the system can generate triple entanglement among the two magnon modes and the atom and also can transfer information from the atom into the two remote YIG spheres. Here, we would like to investigate the simultaneous blockade of two remote magnons by an atom for the two cases discussed above. Including the thermal environment of the atom as well as the two YIG spheres, we can write the master equation of the reduced subsystem as

$$\begin{aligned} \dot{\rho} = & -i[\Delta_m m_i^\dagger m_i + \Delta_a \sigma_+ \sigma_- + \Omega(\sigma_- + \sigma_+), \rho] \\ & + \sum_{i,j=-l,l} -iy_{ij}[m_i^\dagger m_j, \rho] \\ & - iw_{0i}[m_i^\dagger \sigma_- + \sigma_+ m_i, \rho] - iq_{00}[\sigma_+ \sigma_-, \rho] \\ & + x_{ij}(2m_i \rho m_j^\dagger - m_j^\dagger m_i \rho - \rho m_j^\dagger m_i) \\ & + s_{0i}(2\sigma_- \rho m_i^\dagger - m_i^\dagger \sigma_- \rho - \rho m_i^\dagger \sigma_- + \text{H.c.}) \\ & + r_{00}(2\sigma_- \rho \sigma_+ - \sigma_+ \sigma_- \rho - \rho \sigma_+ \sigma_-) \\ & + \sum_{i=-l,l} n_m \kappa_m (2m_i^\dagger \rho m_i - m_i m_i^\dagger \rho - \rho m_i m_i^\dagger) \\ & + \sum_{i=-l,l} (n_m + 1) \kappa_m (2m_i \rho m_i^\dagger - m_i^\dagger m_i \rho - \rho m_i^\dagger m_i) \\ & + n_a \kappa_a (2\sigma_+ \rho \sigma_- - \sigma_- \sigma_+ \rho - \rho \sigma_- \sigma_+) \\ & + (n_a + 1) \kappa_a (2\sigma_- \rho \sigma_+ - \sigma_+ \sigma_- \rho - \rho \sigma_+ \sigma_-), \quad (10) \end{aligned}$$

where the free Hamiltonian H_0 as well as the classical weak pumping H_{drive} are included, κ_m and κ_a are the decay rates for the magnon modes and for the atom, respectively. n_m and n_a are the thermal mean particle numbers of the magnon modes and atom, respectively. Employing the master equation (10),

we can numerically calculate the equal-time second-order correlation function $g_i^2(0) = \frac{\text{Tr}(m_i^\dagger m_i m_i \rho)}{[\text{Tr}(m_i^\dagger m_i \rho)]^2}$ ($i = -l, l$) to describe the nonclassical statistics of magnons. The correlation function $g_i^2(0) > 1$ is referred to as super-Poissonian, $g_i^2(0) = 1$ is referred to as Poissonian, and $g_i^2(0) < 1$ indicates sub-Poissonian (also means antibunching), and the limit $g_i^2(0) \rightarrow 0$ corresponds to the complete blockade.

To make clear the mechanism of magnon blockade, we take the case of outside band ($\Delta_p > 2J$ or $\Delta_p < -2J$) as an example to derive the analytical expression of $g_i^2(0)$, and consider $\kappa_c = 0$, $n_m = n_a = 0$, from (10) we can rewrite the effective Hamiltonian under no count condition [ignoring the jump term $m_i \rho m_i^\dagger$, ($i = -l, l$) and $\sigma_- \rho \sigma_+$] as

$$H_{\text{eff}}' = \sum_{i=-l, l} \Delta_1 m_i^\dagger m_i + \Delta_2 \sigma_+ \sigma_- + \Omega(\sigma_- + \sigma_+) + E(m_{-l}^\dagger m_l + m_l^\dagger m_{-l}) + F(m_i \sigma_+ + \sigma_- m_i^\dagger), \quad (11)$$

where $\Delta_1 = \Delta_m + y_{ll} - i\kappa_m$, $\Delta_2 = \Delta_a + q_{00} - i\kappa_a$, for simplicity, we write $E = y_{-ll}$ and $F = w_{0l}$, which is a non-Hermitian Hamiltonian, the eigenvalues and eigenstates of Eq. (11) are shown in Appendix A. Its eigenvalues are complex numbers, the real parts present the effective frequencies, and the imaginary parts indicate the dissipation of the energy levels so that the bandwidth of the energy levels is extended. Thus, for the case, we can employ the wave function and the eigenvalues to illustrate the mechanism of the blockade of magnons.

In the weak driving limit, the state of the system can be truncated in a few exciting subspaces, which is approximately expressed as

$$|\psi\rangle = C_{g00}|g00\rangle + C_{e00}|e00\rangle + C_{g10}|g10\rangle + C_{g01}|g01\rangle + C_{e10}|e10\rangle + C_{e01}|e01\rangle + C_{g11}|g11\rangle + C_{g02}|g02\rangle + C_{g20}|g20\rangle. \quad (12)$$

The probability amplitude can be obtained by solving the Schrödinger equation $i\frac{\partial}{\partial t}|\psi\rangle = H_{\text{eff}}'|\psi\rangle$. Thus the second-order correlation function of magnons is derived as

$$g_{-l}^2(0) = g_l^2(0) = \frac{2|C_{g20}|^2}{[|C_{g10}|^2 + |C_{e10}|^2 + |C_{g11}|^2 + 2|C_{g20}|^2]^2}. \quad (13)$$

The expressions of the probability amplitude are given in Appendix B. The solution (13) is a steady-state result and has no relevance to the initial state of the system. Because $g_{-l}^2(0)$ is always equal to $g_l^2(0)$, under a certain group of parameters, $g_{-l}^2(0)$ and $g_l^2(0)$ can be both much less than one even approach to zero, we call it a simultaneous blockade.

In Fig. 4, for the case of the outside band, we employ (10) numerically to plot $\log_{10} g_{-l}^2$ as functions of detuning Δ_a with $n_m = n_a = 0$. Figure 4(a) shows that the analytical result of $\log_{10} g_{-l}^2$ using (13) well coincides with that of the numerical result of employing (10), which means that we can use the analytical expression to illustrate the behavior of the second-order correlation function of the magnon. At point A in Fig. 4(a), $\Delta_a = 44.6\kappa_m$, we can calculate $\text{Re}[\lambda_{1+}] = 0$ using the expression (A1) with the parameters in Fig. 4, which means that single-excitation state $|1_+\rangle$ is easily populated, and

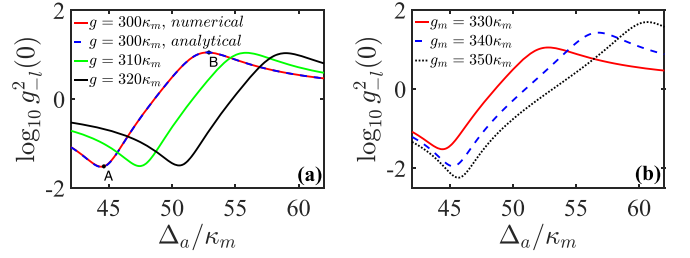


FIG. 4. $\log_{10} g_{-l}^2$ varying with Δ_a for several values of (a) g as well as (b) g_m . For (a), $g_m = 330\kappa_m$, for (b), $g = 300\kappa_m$, for all of the plots, $n' = 4$, $n'' = 2$, $\kappa_m = \kappa_a = 1$, $\Omega = 0.1\kappa_m$, $\kappa_c = 0$, $n_m = n_a = 0$, $\omega_m = 9.3 \times 10^3 \kappa_m$, the other parameters are the same as in Fig. 2.

the higher magnon excitation states $|20\rangle$, $|2_{1\pm}\rangle$, and $|2_{1\pm}\rangle$ are hindered by the dressed state of the atom and the magnon modes, thus the magnon modes exhibit blockade. As Eq. (13) shows, the statistics of magnon $-l$ and magnon l are the same, so $\log_{10} g_{-l}^2 = \log_{10} g_l^2$, a simultaneous blockade of the two magnons at point A can be produced. In addition, with the increasing of g , the detuning Δ_a for $g_{-l}^2(0)$ to achieve an optimal blockade increases. This is because the coupling g directly relates to the frequency shift, see Eqs. (7) and (8). Although a large value of g also means the large effective coupling between the atom and the YIG sphere (see the expression w_{0i}), the effect of the increasing g on reducing $g_{-l}^2(0)$ is depressed due to the frequency shift, it slightly affects the value of $g_{-l}^2(0)$. At point B with $\Delta_a = 52.9\kappa_m$, we can derive $\text{Re}[\lambda_{2+}] = 0$, then the magnon modes exhibit a bunching effect, this is due to the two-magnon state $|2_{1+}\rangle$ populated. Fig. 4(b) shows the $\log_{10} g_{-l}^2$ as functions of detuning Δ_a for several values of g_m . Different from the function of the g on affecting $g_{-l}^2(0)$, although a large value of g_m shifts the frequency of magnon mode, it only slightly shifts the detuning Δ_a but improves the blockade of the magnon mode greatly. This property offers us a method to enhance the blockade of the magnons by improving the coupling between the YIG sphere and the cavity field.

We also would like to point out that the value of the detuning Δ_a for $g_{-l}^2(0)$ to achieve optimal blockade is within the region $44.6\kappa_m - 50.7\kappa_m$ in Fig. 4, comparing with the $\omega_p = 9.25 \times 10^3 \kappa_m$, the frequency of the atom $\omega_a = 9294.6\kappa_m - 9300.7\kappa_m$ is near to the frequency of the classical pumping, that is to say, $|\omega_a - \omega_c| = 2105.4\kappa_m - 2099.3\kappa_m \gg 2J = 1000\kappa_m$, which means the frequency of the atom is far from the center frequency of the band ω_c . So we can infer that the two cases outside and inside band correspond to the frequency of the atom outside and inside the band, respectively. In addition, $\Delta_a = |\omega_a - \omega_c| = 2105.4\kappa_m - 2099.3\kappa_m \gg 2J = 1000\kappa_m$, $\Delta_m = |\omega_m - \omega_c| = 2100\kappa_m \gg 2J$, and $\{g, g_m\} \ll |v_g(\omega_j)|$, which means the frequency of the atom (magnon) is far from the edge of the cavity photon band and the Born-Markov approximation is valid under the group of parameters.

For the case of the frequency of the atom inside band ($-2J < \Delta_p < 2J$), $\log_{10} g_{-l}^2$ as functions of detuning Δ_a is plotted numerically by employing (10) in Fig. 5. The mechanism of the magnon blockade in the current scheme is single excitation resonant no matter if it is the outside or inside band,

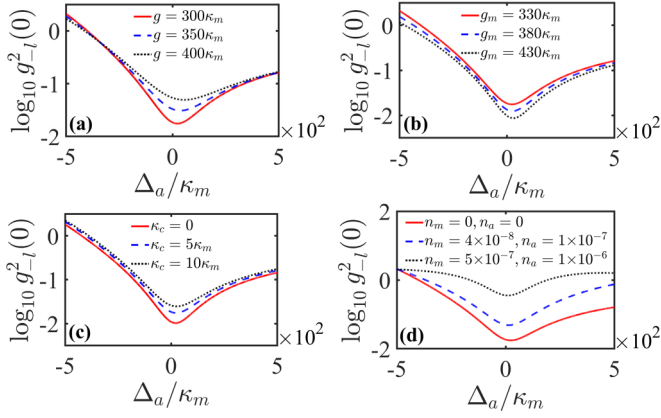


FIG. 5. $\log_{10} g_{-l}^2$ varying with Δ_a for several values of (a) g , (b) g_m , (c) κ_c , and (d) (n_m, n_a) . For (a), $g_m = 330\kappa_m$, for (b), $g = 300\kappa_m$, for (c) and (d), $g = 300\kappa_m$, $g_m = 330\kappa_m$, for (a)–(c), $n_m = n_a = 0$, for (a)–(d), $\kappa_c = 5\kappa_m$, for all of the plots, $n' = 100$, $n'' = 50$, $\kappa_m = \kappa_a = 1$, $\Omega = 0.1\kappa_m$, $\omega_m = 11.2 \times 10^3 \kappa_m$, the other parameters are the same as in Fig. 3.

therefore, the points at which $\log_{10} g_{-l}^2$ achieve minimum values still satisfy the single excitation resonant. However, comparing Fig. 5(a) with Fig. 4(a), the increasing of g on affecting minimum values $\log_{10} g_{-l}^2$ is changed from mainly shifting frequencies into the extended energy level bandwidth (which means increasing the dissipation of the atom). Although g_m also results in a dissipation of the magnon, the increasing of g_m also means the enlargement of the effective coupling between the atom and the YIG sphere, thus, a large value of g_m still benefits the blockade of magnon, see Fig. 5(b), similar to that in Fig. 4(b). The different behavior of increasing g and g_m on affecting $\log_{10} g_{-l}^2$, comparing Fig. 5(a) with Fig. 5(b), is because the dissipation of atom is harmful to the magnon blockade while the dissipation of magnon mode is in favor of the magnon blockade due to the easy population in low level with dissipation. Figure 5(c) shows that the dissipation of the cavity array is harmful to the magnon blockade effect because the dissipation κ_c decreases the coherent and dissipative coupling, see Fig. 3. The thermal noise of the atom as well as the magnon modes, as shown in Fig. 5(d), can break the magnetic blockade. The thermal excitation still needs to be depressed so as to achieve a good blockade for magnon modes. Most importantly, when the detuning is inside the band, the simultaneous blockade of the two magnons can reach a large distance, for example, $n' = 100$ shown in Fig. 5, therefore, the current scheme can simultaneously blockade the two remote magnon modes.

IV. DISCUSSION AND CONCLUSION

The coupled-cavity array is experimentally [51–53] realized to consist of N linearly coupled superconducting transmission line cavities. In [52], the coupled-cavity array was composed of 21 high-impedance microwave resonators. Each resonator consisted of an array of ten Josephson junctions, producing the hopping strength between the nearest cavities $J/2\pi = 249$ MHz. In addition, two artificial atoms are implemented as superconducting flux tunable transmons

capacitively coupled to the array with strength $g_1/2\pi = 338$ MHz and $g_2/2\pi = 311$ MHz, the dissipation of two qubits is $\kappa_a/2\pi \approx 50$ kHz, thus $J = 4980\kappa_a$, $g_1 = 6760\kappa_a$, $g_2 = 6220\kappa_a$, which are much larger than what we use in Figs. 2–5. In [54], the coherent coupling between two remote magnons mediated by a superconducting circuit was realized, where the magnon-photon coupling $g_m = 130\kappa_m$, and in [30], the magnon-photon coupling $g_m = 50.05\kappa_m$; these are still less than what we use in Figs. 2–5. The requirement of the current scheme for the coupling between microwave photons and magnons may be satisfied in the near future. In addition, the coupled-cavity array can also be formed by photonic crystal cavities [60,61], in [60], the resonant coupling interaction in a coupled-cavity photonic crystal molecule can be controlled by using a local and reversible photochromic tuning technique. In [61], two atoms were coupled to the photonic crystals with the strength of $g = 2000\kappa_a$, which was much larger than what we used in Figs. 2–5. For magnons and optical photons coupling [62,63], it is a three-wave optomagnetic interaction, which can be linearized [64] because one of the modes is driven by a classical field, thus the optomagnetic coupling is adjustable. Therefore, our model may be realized in a cavity array composed of photonic crystal cavities.

In this paper, we present a scheme to simultaneously blockade two remote magnons by coupling them to an odd-number cavity array where an atom is contained in the middle cavity, and two YIG spheres are placed symmetrically to the atom. By eliminating the cavity array, the effective coherent and dissipative couplings among the two magnons and the atom are obtained. In the case of the frequency of the atom outside the band, the dissipative couplings disappear, and only coherent couplings survive, thus putting an atom in the middle of two magnons is equivalent to coupling a giant atom to them. However, the effective dispersive couplings decrease rapidly with the increasing of the distance between two YIG spheres. However, in the case of the frequency of the atom inside band, although the induced dissipation cannot be eliminated, the dissipative coupling and the coherent coupling can coexist for remote two YIG spheres. We further show that, under the condition of single excitation resonance, the simultaneous blockade of two remote magnons can be realized, but the magnetic and atomic thermal noise is still required to be depressed.

ACKNOWLEDGMENTS

This work is supported by the National Natural Science Foundation of China under Grant No. 12274053 and National Key R&D Program of China (Grant No. 2021YFE0193500).

APPENDIX A: EIGENVALUES AND EIGENSTATES OF THE EQ. (11)

The H'_{eff} has nine eigenvalues, which are

$$\begin{aligned} \lambda_0 &= 0, \\ \lambda_{10} &= \Delta_1 - E, \\ \lambda_{20} &= 2(\Delta_1 - E), \\ \lambda_{1+} &= \frac{\Delta_1 + \Delta_2 + E}{2} + \frac{P_1}{2}, \end{aligned}$$

$$\begin{aligned}
\lambda_{1-} &= \frac{\Delta_1 + \Delta_2 + E}{2} - \frac{P_1}{2}, \\
\lambda_{2_{1+}} &= \frac{3\Delta_1 + \Delta_2 - E}{2} + \frac{P_1}{2}, \\
\lambda_{2_{1-}} &= \frac{3\Delta_1 + \Delta_2 - E}{2} - \frac{P_1}{2}, \\
\lambda_{2_{2+}} &= \frac{3\Delta_1 + \Delta_2 + 3E}{2} + \frac{P_2}{2}, \\
\lambda_{2_{2-}} &= \frac{3\Delta_1 + \Delta_2 + 3E}{2} - \frac{P_2}{2},
\end{aligned} \tag{A1}$$

where $P_1 = \sqrt{Q^2 + 8F^2}$, $P_2 = \sqrt{Q^2 + 16F^2}$ with $Q = \Delta_1 - \Delta_2 + E$.

In addition, the corresponding eigenstates are

$$\begin{aligned}
|0\rangle &= |g00\rangle, \\
|10\rangle &= -\frac{1}{\sqrt{2}}|g10\rangle + \frac{1}{\sqrt{2}}|g01\rangle, \\
|20\rangle &= -\frac{1}{\sqrt{2}}|g11\rangle + \frac{1}{2}|g02\rangle + \frac{1}{2}|g20\rangle, \\
|1_+\rangle &= \frac{1}{T_1} \left[(P_1 - Q)2F|e00\rangle + 4F^2|g10\rangle + 4F^2|g01\rangle \right], \\
|1_-\rangle &= \frac{1}{T_2} \left[-(P_1 + Q)2F|e00\rangle + 4F^2|g10\rangle + 4F^2|g01\rangle \right], \\
|2_{1+}\rangle &= \frac{1}{T_3} [2\sqrt{2}F(P_1 - Q)|e10\rangle \\
&\quad - 2\sqrt{2}F(P_1 - Q)|e01\rangle - 8F^2|g02\rangle + 8F^2|g20\rangle], \\
|2_{1-}\rangle &= \frac{1}{T_4} [-2\sqrt{2}F(P_1 + Q)|e10\rangle \\
&\quad + 2\sqrt{2}F(P_1 + Q)|e01\rangle - 8F^2|g02\rangle + 8F^2|g20\rangle], \\
|2_{2+}\rangle &= \frac{1}{T_5} [2\sqrt{2}F(P_2 - Q)|e10\rangle + 2\sqrt{2}F(P_2 - Q)|e01\rangle \\
&\quad + 8\sqrt{2}F^2|g11\rangle + 8F^2|g02\rangle + 8F^2|g20\rangle], \\
|2_{2-}\rangle &= \frac{1}{T_6} [-2\sqrt{2}F(P_2 - Q)|e10\rangle - 2\sqrt{2}F(P_2 + Q)|e01\rangle \\
&\quad + 8\sqrt{2}F^2|g11\rangle + 8F^2|g02\rangle + 8F^2|g20\rangle],
\end{aligned} \tag{A2}$$

where $T_1 = (P_1 - Q)^2 + 8F^2$, $T_2 = (P_1 + Q)^2 + 8F^2$, $T_3 = 2(P_1 - Q)^2 + 16F^2$, $T_4 = 2(P_1 + Q)^2 + 16F^2$, $T_5 = 2(P_2 - Q)^2 + 32F^2$, $T_6 = 2(P_2 + Q)^2 + 32F^2$.

APPENDIX B: STEADY-STATE SOLUTION OF PROBABILITY AMPLITUDE

By solving the Schrödinger equation $i\frac{\partial}{\partial t}|\psi\rangle = H'_{\text{eff}}|\psi\rangle$, the dynamic evolution of the probability amplitude is obtained

$$\begin{aligned}
i\dot{C}_{g00} &= 0, \\
i\dot{C}_{e00} &= \Delta_2 C_{e00} + FC_{g10} + FC_{g01} + \Omega C_{g00}, \\
i\dot{C}_{g10} &= \Delta_1 C_{g10} + EC_{g01} + FC_{e00}, \\
i\dot{C}_{g01} &= \Delta_1 C_{g01} + EC_{g10} + FC_{e00}, \\
i\dot{C}_{e10} &= \Delta_1 C_{e10} + \Delta_2 C_{e10} + EC_{e01} + \sqrt{2}FC_{g20} \\
&\quad + FC_{g11} + \Omega C_{g10}, \\
i\dot{C}_{e01} &= \Delta_1 C_{e01} + \Delta_2 C_{e01} + EC_{e10} + \sqrt{2}FC_{g02} \\
&\quad + FC_{g11} + \Omega C_{g01}, \\
i\dot{C}_{g11} &= 2\Delta_1 C_{g11} + \sqrt{2}EC_{g02} + \sqrt{2}EC_{g20} \\
&\quad + FC_{e01} + FC_{e10}, \\
i\dot{C}_{g02} &= 2\Delta_1 C_{g02} + \sqrt{2}EC_{g11} + \sqrt{2}FC_{e01}, \\
i\dot{C}_{g20} &= 2\Delta_1 C_{g20} + \sqrt{2}EC_{g11} + \sqrt{2}FC_{e10},
\end{aligned} \tag{B1}$$

where the jumping from high level to low level is ignored, as was done in [65]. The steady-state solution of Eq. (B1) is

$$\begin{aligned}
C_{g11} &= \frac{F^2\Omega^2}{Z_1}, \\
C_{g20} = C_{g02} &= \frac{F^2\Omega^2}{\sqrt{2}Z_1}, \\
C_{e01} = C_{e10} &= \frac{-F(\Delta_1 + E)\Omega^2}{Z_1}, \\
C_{e00} &= \frac{-(\Delta_1 + E)\Omega}{\Delta_2(\Delta_1 + E) - 2F^2}, \\
C_{g01} = C_{g10} &= \frac{F\Omega}{\Delta_2(\Delta_1 + E) - 2F^2},
\end{aligned} \tag{B2}$$

where $Z_1 = \Delta_2(\Delta_1 + E)^2(\Delta_1 + \Delta_2 + E) - 2(\Delta_1 + E)(\Delta_1 + 2\Delta_2 + E)F^2 + 4F^4$.

- [1] J.-F. Huang, J.-Q. Liao, and C. P. Sun, Photon blockade induced by atoms with Rydberg coupling, *Phys. Rev. A* **87**, 023822 (2013).
- [2] W.-W. Deng, G.-X. Li, and H. Qin, Enhancement of the two-photon blockade in a strong-coupling qubit-cavity system, *Phys. Rev. A* **91**, 043831 (2015).
- [3] C. J. Zhu, Y. P. Yang, and G. S. Agarwal, Collective multiphoton blockade in cavity quantum electrodynamics, *Phys. Rev. A* **95**, 063842 (2017).
- [4] C. Lang, D. Bozyigit, C. Eichler, L. Steffen, J. M. Fink, A. A. Abdumalikov, M. Baur, S. Filipp, M. P. da Silva, A. Blais, and A. Wallraff, Observation of resonant photon blockade at

- microwave frequencies using correlation function measurements, *Phys. Rev. Lett.* **106**, 243601 (2011).
- [5] K. M. Birnbaum, A. Boca, R. Miller, A. D. Boozer, T. E. Northup, and H. J. Kimble, Photon blockade in an optical cavity with one trapped atom, *Nature (London)* **436**, 87 (2005).
- [6] A. Imamoglu, H. Schmidt, G. Woods, and M. Deutsch, Strongly interacting photons in a nonlinear cavity, *Phys. Rev. Lett.* **79**, 1467 (1997).
- [7] A. Miranowicz, M. Paprzycka, Y.-X. Liu, J. Bajer, and F. Nori, Two-photon and three-photon blockades in driven nonlinear systems, *Phys. Rev. A* **87**, 023809 (2013).

- [8] J.-Q. Liao and F. Nori, Photon blockade in quadratically coupled optomechanical systems, *Phys. Rev. A* **88**, 023853 (2013).
- [9] H. J. Sniijders, J. A. Frey, J. Norman, H. Flayac, V. Savona, A. C. Gossard, J. E. Bowers, M. P. van Exter, D. Bouwmeester, and W. Löffler, Observation of the unconventional photon blockade, *Phys. Rev. Lett.* **121**, 043601 (2018).
- [10] C. Vaneph, A. Morvan, G. Aiello, M. Féchant, M. Aprili, J. Gabelli, and J. Estève, Observation of the unconventional photon blockade in the microwave domain, *Phys. Rev. Lett.* **121**, 043602 (2018).
- [11] H. Flayac and V. Savona, Unconventional photon blockade, *Phys. Rev. A* **96**, 053810 (2017).
- [12] D. Gerace and V. Savona, Unconventional photon blockade in doubly resonant microcavities with second-order nonlinearity, *Phys. Rev. A* **89**, 031803(R) (2014).
- [13] M.-A. Lemonde, N. Didier, and A. A. Clerk, Antibunching and unconventional photon blockade with Gaussian squeezed states, *Phys. Rev. A* **90**, 063824 (2014).
- [14] Y. H. Zhou, H. Z. Shen, and X. X. Yi, Unconventional photon blockade with second-order nonlinearity, *Phys. Rev. A* **92**, 023838 (2015).
- [15] B. Sarma and A. K. Sarma, Unconventional photon blockade in three-mode optomechanics, *Phys. Rev. A* **98**, 013826 (2018).
- [16] H. Z. Shen, Q. Wang, J. Wang, and X. X. Yi, Nonreciprocal unconventional photon blockade in a driven dissipative cavity with parametric amplification, *Phys. Rev. A* **101**, 013826 (2020).
- [17] J. A. Haigh, S. Langenfeld, N. J. Lambert, J. J. Baumberg, A. J. Ramsay, A. Nunnenkamp, and A. J. Ferguson, Magneto-optical coupling in whispering-gallery-mode resonators, *Phys. Rev. A* **92**, 063845 (2015).
- [18] A. Osada, A. Gloppe, R. Hisatomi, A. Noguchi, R. Yamazaki, M. Nomura, Y. Nakamura, and K. Usami, Brillouin light scattering by magnetic quasivortices in cavity optomagnonics, *Phys. Rev. Lett.* **120**, 133602 (2018).
- [19] T. S. Parvini, V. A. S. V. Bittencourt, and S. V. Kusminskiy, Antiferromagnetic cavity optomagnonics, *Phys. Rev. Res.* **2**, 022027(R) (2020).
- [20] S. V. Kusminskiy, Cavity optomagnonics, in *Optomagnonic Structures: Novel Architectures for Simultaneous Control of Light and Spin Waves* (World Scientific, Singapore, 2021), pp. 299–353.
- [21] C. A. Potts, E. Varga, V. A. S. V. Bittencourt, S. V. Kusminskiy, and J. P. Davis, Dynamical backaction magnomechanics, *Phys. Rev. X* **11**, 031053 (2021).
- [22] X. Zhang, C.-L. Zou, L. Jiang, and H. X. Tang, Cavity magnomechanics, *Sci. Adv.* **2**, e1501286 (2016).
- [23] Y. Tabuchi, S. Ishino, A. Noguchi, T. Ishikawa, R. Yamazaki, K. Usami, and Y. Nakamura, Coherent coupling between a ferromagnetic magnon and a superconducting qubit, *Science* **349**, 405 (2015).
- [24] Y. Tabuchi, S. Ishino, A. Noguchi, T. Ishikawa, R. Yamazaki, K. Usami, and Y. Nakamura, Quantum magnonics: The magnon meets the superconducting qubit, *C. R. Phys.* **17**, 729 (2016).
- [25] D. Lachance-Quirion, S. P. Wolski, Y. Tabuchi, S. Kono, K. Usami, and Y. Nakamura, Entanglement-based single-shot detection of a single magnon with a superconducting qubit, *Science* **367**, 425 (2020).
- [26] Y. Tabuchi, S. Ishino, T. Ishikawa, R. Yamazaki, K. Usami, and Y. Nakamura, Hybridizing ferromagnetic magnons and microwave photons in the quantum limit, *Phys. Rev. Lett.* **113**, 083603 (2014).
- [27] X. Zhang, C.-L. Zou, L. Jiang, and H. X. Tang, Strongly coupled magnons and cavity microwave photons, *Phys. Rev. Lett.* **113**, 156401 (2014).
- [28] J. T. Hou and L. Liu, Strong coupling between microwave photons and nanomagnet magnons, *Phys. Rev. Lett.* **123**, 107702 (2019).
- [29] J. Bourhill, N. Kostylev, M. Goryachev, D. L. Creedon, and M. E. Tobar, Ultrahigh cooperativity interactions between magnons and resonant photons in a YIG sphere, *Phys. Rev. B* **93**, 144420 (2016).
- [30] A. Ghirri, C. Bonizzoni, M. Maksutoglu, A. Mercurio, O. Di Stefano, S. Savasta, and M. Affronte, Ultrastrong magnon-photon coupling achieved by magnetic films in contact with superconducting resonators, *Phys. Rev. Appl.* **20**, 024039 (2023).
- [31] J.-K. Xie, S.-L. Ma, and F.-L. Li, Quantum-interference-enhanced magnon blockade in an yttrium-iron-garnet sphere coupled to superconducting circuits, *Phys. Rev. A* **101**, 042331 (2020).
- [32] X. Li, X. Wang, Z. Wu, W.-X. Yang, and A. Chen, Tunable magnon antibunching in a hybrid ferromagnet-superconductor system with two qubits, *Phys. Rev. B* **104**, 224434 (2021).
- [33] K. Wu, W.-X. Zhong, G.-L. Cheng, and A.-X. Chen, Phase-controlled multimagnon blockade and magnon-induced tunneling in a hybrid superconducting system, *Phys. Rev. A* **103**, 052411 (2021).
- [34] Y. Wang, W. Xiong, Z. Xu, G.-Q. Zhang, and J.-Q. You, Dissipation-induced nonreciprocal magnon blockade in a magnon-based hybrid system, *Sci. China Phys. Mech. Astron.* **65**, 260314 (2022).
- [35] Y.-J. Xu, T.-L. Yang, L. Lin, and J. Song, Conventional and unconventional magnon blockades in a qubit-magnon hybrid quantum system, *J. Opt. Soc. Am. B* **38**, 876 (2021).
- [36] A. Parai, D. Ganthya, and P. C. Jana, Unconventional magnon blockade in a superconducting qubit coupled magnomechanical system, *Eur. Phys. J. D* **77**, 40 (2023).
- [37] M. S. Kheirabady, E. Ghasemian, and M. K. Tavassoly, Magnon blockade and magnon-atom entanglement induced by a qutrit coupled to a ferromagnetic YIG sphere, *Ann. Phys. (Leipzig)* **535**, 2300024 (2023).
- [38] Z.-X. Liu, H. Xiong, and Y. Wu, Magnon blockade in a hybrid ferromagnet-superconductor quantum system, *Phys. Rev. B* **100**, 134421 (2019).
- [39] L. Wang, Z.-X. Yang, Y.-M. Liu, C.-H. Bai, D.-Y. Wang, S. Zhang, and H.-F. Wang, Magnon blockade in a \mathcal{PT} -symmetric-like cavity magnomechanical system, *Ann. Phys. (Leipzig)* **532**, 2000028 (2020).
- [40] F. Wang, C. Gou, J. Xu, and C. Gong, Hybrid magnon-atom entanglement and magnon blockade via quantum interference, *Phys. Rev. A* **106**, 013705 (2022).
- [41] C. Zhao, X. Li, S. Chao, R. Peng, C. Li, and L. Zhou, Simultaneous blockade of a photon, phonon, and magnon induced by a two-level atom, *Phys. Rev. A* **101**, 063838 (2020).
- [42] A. Metelmann and A. A. Clerk, Nonreciprocal photon transmission and amplification via reservoir engineering, *Phys. Rev. X* **5**, 021025 (2015).
- [43] M. Harder, Y. Yang, B. M. Yao, C. H. Yu, J. W. Rao, Y. S. Gui, R. L. Stamps, and C.-M. Hu, Level attraction due to

- dissipative magnon-photon coupling, *Phys. Rev. Lett.* **121**, 137203 (2018).
- [44] B. Yao, T. Yu, X. Zhang, W. Lu, Y. Gui, C.-M. Hu, and Y. M. Blanter, The microscopic origin of magnon-photon level attraction by traveling waves: Theory and experiment, *Phys. Rev. B* **100**, 214426 (2019).
- [45] P.-C. Xu, J. W. Rao, Y. S. Gui, X. Jin, and C.-M. Hu, Cavity-mediated dissipative coupling of distant magnetic moments: Theory and experiment, *Phys. Rev. B* **100**, 094415 (2019).
- [46] Y.-P. Wang, J. W. Rao, Y. Yang, P.-C. Xu, Y. S. Gui, B. M. Yao, J. Q. You, and C.-M. Hu, Nonreciprocity and unidirectional invisibility in cavity magnonics, *Phys. Rev. Lett.* **123**, 127202 (2019).
- [47] J. Zou, S. Bosco, E. Thingstad, J. Klinovaja, and D. Loss, Dissipative spin-wave diode and nonreciprocal magnonic amplifier, *Phys. Rev. Lett.* **132**, 036701 (2024).
- [48] Y. Tserkovnyak, Exceptional points in dissipatively coupled spin dynamics, *Phys. Rev. Res.* **2**, 013031 (2020).
- [49] T. Yu, J. Zou, B. Zeng, J. W. Rao, and K. Xia, Non-Hermitian topological magnonics, [arXiv:2306.04348](https://arxiv.org/abs/2306.04348).
- [50] L. Zhou, Z. R. Gong, Y.-X. Liu, C. P. Sun, and F. Nori, Controllable scattering of a single photon inside a one-dimensional resonator waveguide, *Phys. Rev. Lett.* **101**, 100501 (2008).
- [51] M. Fitzpatrick, N. M. Sundaresan, A. C. Y. Li, J. Koch, and A. A. Houck, Observation of a dissipative phase transition in a one-dimensional circuit QED lattice, *Phys. Rev. X* **7**, 011016 (2017).
- [52] M. Scigliuzzo, G. Calajò, F. Ciccarello, D. P. Lozano, A. Bengtsson, P. Scarlino, A. Wallraff, D. Chang, P. Delsing, and S. Gasparinetti, Controlling atom-photon bound states in an array of Josephson-junction resonators, *Phys. Rev. X* **12**, 031036 (2022).
- [53] D. L. Underwood, W. E. Shanks, J. Koch, and A. A. Houck, Low-disorder microwave cavity lattices for quantum simulation with photons, *Phys. Rev. A* **86**, 023837 (2012).
- [54] Y. Li, V. G. Yefremenko, M. Lisovenko, C. Trevillian, T. Polakovic, T. W. Cecil, P. S. Barry, J. Pearson, R. Divan, V. Tyberkevych, C. L. Chang, U. Welp, W.-K. Kwok, and V. Novosad, Coherent coupling of two remote magnonic resonators mediated by superconducting circuits, *Phys. Rev. Lett.* **128**, 047701 (2022).
- [55] G. Calajò, F. Ciccarello, D. Chang, and P. Rabl, Atom-field dressed states in slow-light waveguide QED, *Phys. Rev. A* **93**, 033833 (2016).
- [56] H. Y. Yuan, W. P. Sterk, A. Kamra, and R. A. Duine, Master equation approach to magnon relaxation and dephasing, *Phys. Rev. B* **106**, 224422 (2022).
- [57] J. Zou, S. Zhang, and Y. Tserkovnyak, Bell-state generation for spin qubits via dissipative coupling, *Phys. Rev. B* **106**, L180406 (2022).
- [58] H. Y. Yuan, W. P. Sterk, A. Kamra, and R. A. Duine, Pure dephasing of magnonic quantum states, *Phys. Rev. B* **106**, L100403 (2022).
- [59] M. O. Scully, M. S. Zubairy, and P. W. Milonni, Quantum optics, *Phys. Today* **51**(10), 90 (1998).
- [60] T. Cai, R. Bose, G. S. Solomon, and E. Waks, Controlled coupling of photonic crystal cavities using photochromic tuning, *Appl. Phys. Lett.* **102**, 141118 (2013).
- [61] J. S. Douglas, H. Habibian, C.-L. Hung, A. V. Gorshkov, H. J. Kimble, and D. E. Chang, Quantum many-body models with cold atoms coupled to photonic crystals, *Nat. Photonics* **9**, 326 (2015).
- [62] A. Osada, R. Hisatomi, A. Noguchi, Y. Tabuchi, R. Yamazaki, K. Usami, M. Sadgrove, R. Yalla, M. Nomura, and Y. Nakamura, Cavity optomagnonics with spin-orbit coupled photons, *Phys. Rev. Lett.* **116**, 223601 (2016).
- [63] J. A. Haigh, A. Nunnenkamp, A. J. Ramsay, and A. J. Ferguson, Triple-resonant Brillouin light scattering in magneto-optical cavities, *Phys. Rev. Lett.* **117**, 133602 (2016).
- [64] H. Xie, Z.-G. Shi, L.-W. He, X. Chen, C.-G. Liao, and X.-M. Lin, Proposal for a Bell test in cavity optomagnonics, *Phys. Rev. A* **105**, 023701 (2022).
- [65] P. Kómár, S. D. Bennett, K. Stannigel, S. J. M. Habraken, P. Rabl, P. Zoller, and M. D. Lukin, Single-photon nonlinearities in two-mode optomechanics, *Phys. Rev. A* **87**, 013839 (2013).